A EUROPEAN JOURNAL

CHEMPHYSCHEM

OF CHEMICAL PHYSICS AND PHYSICAL CHEMISTRY

Accepted Article

Title: Cytosine radical cation: a gas-phase study combining IRMPD spectroscopy, UV-PD spectroscopy, ion-molecule reactions, and theoretical calculations

Authors: Michael Lesslie, John T Lawler, Andy Dang, Joseph A Korn, Daniel Bim, Vincent Steinmetz, Philippe Maitre, Frantisek Turecek, and Victor Ryzhov

To be cited as: *ChemPhysChem* 10.1002/cphc.201700281

Link to VoR: http://dx.doi.org/10.1002/cphc.201700281

A Journal of

ChemPubSoc Europe

WILEY-VCH

www.chemphyschem.org

Cytosine radical cation: a gas-phase study combining IRMPD spectroscopy, UV-PD spectroscopy, ion-molecule reactions, and theoretical calculations

Michael Lesslie,[a] John T. Lawler,[a] Andy Dang,[b] Joseph A. Korn,[b] Daniel Bím,[c] Vincent Steinmetz,[d] Philippe Maître,[d] Frantisek Tureček*[b] and Victor Ryzhov*[a]

Abstract: The radical cation of cytosine ($Cyt^{\bullet+}$) was generated via dissociative oxidation from a ternary Cu(II) complex in the gas phase. The radical cation was characterized by infrared multiple photon dissociation (IRMPD) spectroscopy in the fingerprint region, UV-VIS photodissociation (UV-PD), ion-molecule reactions, and theoretical calculations (density functional theory and ab initio). The IRMPD experimental spectrum has diagnostic bands for two enol/amino and two keto/amino tautomers of $Cyt^{\bullet+}$, that were calculated to be among the lowest-energy isomers in concert with a previous work (J. Wolken, *et al.*, *Int. J. Mass Spectrom.* **2007**). While UV-PD action spectrum can also be matched to a combination of the four lowest-energy tautomers, it does not rule out the presence of a non-classical distonic radical cation. Its formation is, however, unlikely due to the high energy of this isomer and the respective ternary Cu(II) complex. Gas-phase ion-molecule reactions showed that $Cyt^{\bullet+}$ undergoes hydrogen atom abstraction from *n*-propyl thiol, radical recombination reactions with nitric oxide, and electron transfer from dimethyl disulfide.

Introduction

The building blocks of DNA are susceptible to undesired chemical modifications that may result in loss or change of function.[1] For nucleobases, radical formation via oxidative chemical reactions or ionizing radiation is of particular concern as such modifications can have particularly severe consequences such as strand breaks, mutagenesis, and cancer.[2] Whether direct, (radiation induced) or indirect (via chemical reaction), oxidation often results in the formation of a nucleobase radical cation within the DNA strand.[3] This species undergoes a variety of reactions.[4] Most notably, charge transfer via electron hole-migration is followed by proton transfer which disrupts the hydrogen bonding network leading to eventual strand scission.[4]

It is notable that the local environment experienced by nucleobases within DNA is different from model systems in water. In that regard, gas-phase data can be useful in providing insight into intrinsic chemistry of the often-transient nucleobase radicals. Such solvent-free analysis is unencumbered by multi-conformational averaging and counterion effects, allowing for direct experimental observation of the specific radical species.

Multiple gas-phase studies have been devoted to the charged even-electron species of nucleobases and nucleosides in an attempt to uncover the intrinsic structure and properties of the DNA building blocks. Early mass spectrometry based characterization methods, such as kinetic methods, lacked the ability to accurately discriminate between the multiple low-energy structures which are possible for the nucleobases and nucleosides. However, they were successful in characterization of properties such as proton affinity,[5] and metal-binding energetics.[6] Likewise, ion-mobility mass spectrometry (IM-MS) was successful in the characterization of the conformational shapes of oligonucleotides,[7] dinucleotides,[8] and mononucleotides.[9] Such IM-MS studies, which focus on large flexible species, are unfortunately unable to resolve the nucleobase conformers due to their similar cross sectional area.

The development of infrared multiple photon dissociation (IRMPD) spectroscopy, in combination with computational chemistry, presented a novel step forward for the direct structural observation of gas phase ions, and has been leveraged extensively for the structural elucidation of the DNA constituents. Maître, Salpin, and co-workers originally determined the protonated structure of the gas-phase pyrimidine nucleobases to be predominantly the lowest energy enol/amino form with only minor contributions of the keto/amino tautomer.[10] This work was quickly followed by the analysis of monohydrated nucleobases.[11] Since those initial studies, IRMPD spectroscopy has been utilized to examine a multitude of species related to DNA constituents, including, nucleosides,[12] nucleotides,[13] nucleobase dimers,[14] and metal-bound species.[15]

Significantly less work has been done, however, on the examination of one-electron oxidation products of DNA and its

[a] M. Lesslie, J. T. Lawler, V. Ryzhov*
Department of Chemistry and Biochemistry
Northern Illinois University
DeKalb, IL 60115, USA
Email: ryzhov@niu.edu
[b] A. Dang, J. A. Korn, F. Tureček*
Department of Chemistry
University of Washington
Bagley Hall, Box 351700
Seattle, Washington 98195, USA
Email: turecek@chem.washington.edu
[c] D. Bím
Institute of Organic Chemistry and Biochemistry
Academy of Sciences of the Czech Republic
166 10 Prague 6, Czech Republic
[d] V. Steinmetz, P. Maître
Laboratoire de Chimie Physique
Université Paris-Sud
UMR8000 CNRS
91405 Orsay, France

Supporting information for this article is given via a link at the end of the document.

constituents (i.e., nucleobase radical cations) in the gas phase. This first instances revolved around the use of the high-energy electron impact (EI) ionization method to study the fragmentation pathways of the nucleobase radical cations.[16] Neutralization-reionization mass spectrometry (NR-MS) has been used in combination with high-level theoretical calculations to model, study the energetics, and examine the probable structures of the nucleobases and their corresponding radical cations.[17] Most recently, a mixture of cytosine radical cation isomers has been produced by synchrotron-based VUV photoionization of gas-phase cytosine produced in a molecular beam and characterized by ionization energy measurements that were in accord with high-level ab initio calculations.[18]

An alternative nucleobase radical cation generation method was required to be compatible with the mass spectrometers used for gas-phase spectroscopic methods. Dissociation of ternary copper complexes under collision-induced dissociation conditions in ion traps was originally shown to generate singly-charged radical cations of peptides (Eq. 1).[19] Subsequently, this method was extended to the generation of nucleobase and nucleoside radical cations.[20] Using this technique, O'Hair and co-workers were able to successfully determine the tautomeric form of the substituted nucleobase 9-methyl guanine radical cation,[21] as well as the nucleoside deoxyguanosine radical cation, via IRMPD spectroscopy.[22]

$$[Cu^{II}(terpy)(M)]^{\bullet 2+} \rightarrow [Cu^{I}(terpy)]^{+} + M^{\bullet +} \qquad \text{(Eq. 1)}$$

While these studies demonstrate the applicability of gas-phase spectroscopic techniques in defining the native structure of the DNA constituents, the structures of the unsubstituted nucleobase radical cations in the gas phase formed via oxidative dissociation are yet to be determined.

The current work focuses on defining the gas-phase conformational composition of the radical cation of cytosine. Protonated cytosine was found to be a mixture of the two lowest energy tautomers, the enol/amino and keto/amino species **B** and **C** (Scheme 1), both formed via protonation of the most stable neutral species **A** (conventional numbering used throughout this work is shown in red).[10, 11b]

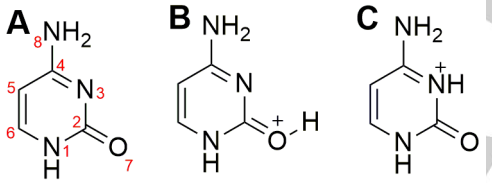

Scheme 1. Low energy tautomers of Cyt (**A**) and protonated Cyt (**B** & **C**).

In an effort to define the specific tautomeric mixture protonated cytosine ions were hydrated in the gas phase. The water molecule attachment significantly lowered the dissociation barrier and allowed for observation of the species in the N-H/O-H stretch region.[11b] Such an approach, however, is not easily implemented for the radical cation of cytosine, which has to be formed via CID inside the ion trap. To avoid such complication, we complement the IRMPD spectroscopy of the cytosine radical cation with the higher-energy single-photon technique, UV-PD action spectroscopy. Gas-phase spectroscopic experiments in this range have previously been utilized for the protonated and monohydrated forms of thymine and uracil.[23] Ion-molecule reactions (IMR) are carried out with various neutrals in order to further examine the chemistry of the cytosine radical cation. Computational chemistry methods are utilized to evaluate low-energy conformations and estimate theoretical absorbance bands.

Results and Discussion

Cytosine radical cation isomers

When the nucleobases are bound within a DNA strand, the hydrogen bonding network of the Watson-Crick pairing results in highly-favored tautomeric conformations of each base. For cytosine, the keto/amino form is preferred. However, the free nucleobases can possess a number of different tautomeric forms. The neutral cytosine molecule has seven formal tautomers (Scheme 2) from which one-electron oxidation would result in independent radical cations of the nucleobase. When considering these seven tautomers computationally, rotational isomers must also be taken into account, resulting in fifteen possible radical cation species of cytosine (Figure S1).

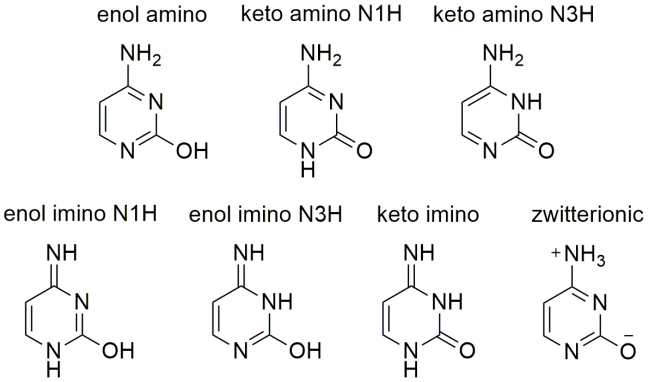

Scheme 2. The seven tautomers of neutral Cyt.

The relative energetics of the cytosine tautomeric forms have previously been determined computationally, both as a neutral species and as radical cations.[11b, 17g] Herein, the cytosine radical cation was initially explored at the B3LYP/6311++G(d,p) level of theory. This approach was found to reproduce the relative energy rankings of the low-energy tautomers at the highest level of theory previously used, CCSD(T)/6-311++G(3df,2p), with only minor exceptions (notably species **3,** corresponding to the keto amino N1H tautomer**,** is found ~ 5 kJ mol^{-1} higher in energy at both the CCSD(T)/6-311++G(3df,2p) and CCSD(T)/aug-cc-pVTZ level of theory).[17g]

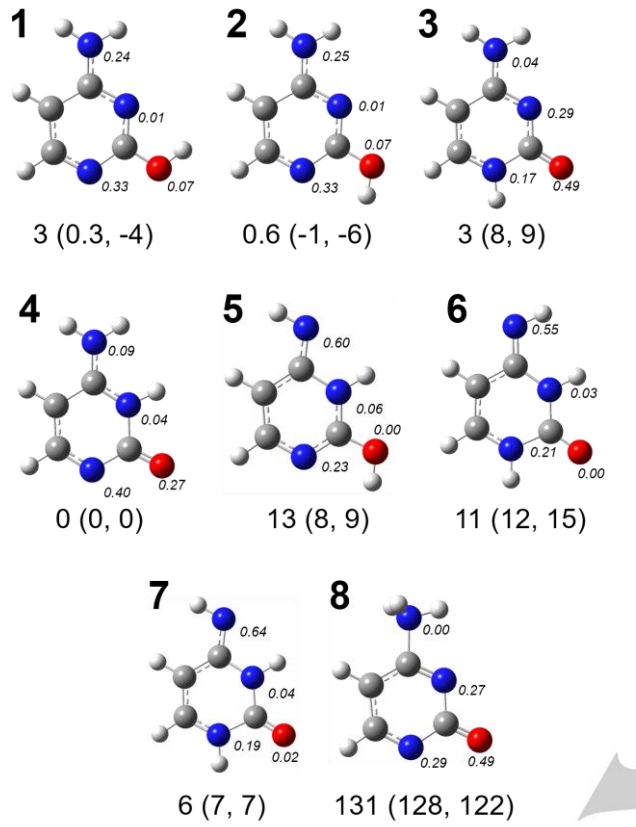

Figure 1. Optimized structures of the cytosine radical cation at the B3LYP/6-311++G(d,p) level of theory. Relative energies calculated at that level are displayed including zero-point vibrational energies and referring to 0 K in kJ mol^{-1} (CCSD(T)/6-311++G(3f,2p)[17g] and CCSD(T)/aug-cc-pVTZ are given in parentheses for comparison). The spin electron density on heteroatoms is shown in italics.

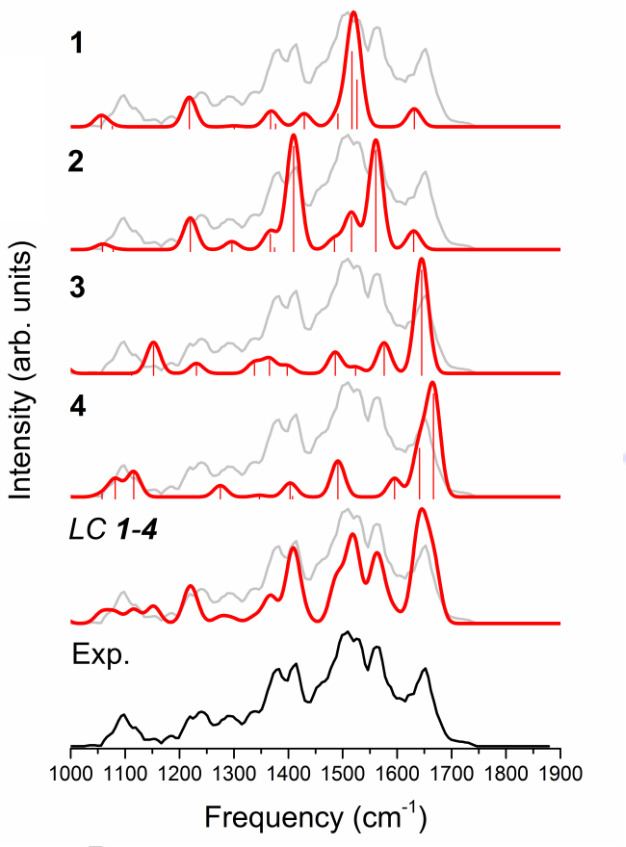

Figure 2. Experimental (black/gray) and theoretically calculated (red) IR spectra of the four lowest energy cytosine radical cations (**1**-**4**). The linear combination (*LC* ***1-4***) is based on equal parts of each isomer. Theoretical spectra were calculated at the B3LYP/6-311++G(d,p) level of theory with the FWHM set to 30 cm^{-1} and scaled using a factor of 0.98.

In fact, the same seven species are predicted within 15 kJ mol^{-1} of the lowest energy conformer by both computational methods (Figure 1, **1**-**7**). Of these species, all isomers possessing the amino form (**1**-**4**) and isomer **7** were found within 10 kJ mol^{-1} of the reference isomer **4**. All other structures were found to be higher in energy (see Figure S1).

Gas-phase action spectroscopy – IRMPD

The infrared multiple photon dissociation (IRMPD) action spectrum was collected in the "fingerprint region" (1000 – 1900 cm^{-1}) for the cytosine radical cation. The experimental spectrum for the cytosine radical cation reveals eight notable peaks (Figure 2 and Table 1). Based on the number of observed bands alone, it is unlikely that the profile corresponds to a single isomeric species in the gas phase. Comparison to the theoretically calculated absorbance bands for each of the seven low-energy isomers confirms the lack of a mono-isomeric match (Figure 2, see Figure S3 for the simulated IR of all remaining cytosine radical structures). In particular, the calculated keto/imino tautomers (**6** and **7**) have a strong absorbance near 1850 cm^{-1}, corresponding to the C=O stretching motion, which is absent from the experimental spectrum (Figure S3). The enol/imino with a proton at the N3 position (**5**) also displays a poor match to the experimental spectrum (Figure S3). Combined with the tautomer existing at over 10 kJ mol^{-1} higher energy than the lowest energy isomer at both levels of theory, it is unlikely that this species is present in any substantial population under equilibrium conditions. The four remaining amino-type isomers (**1**-**4**) were found to be the lowest in energy when calculated using the B3LYP/6311++G(d,p) level of theory (within 3 kJ mol^{-1}, Figure 1). This energy difference is small enough to consider that these isomers will be populated. The experimentally observed spectrum (Figure 2) clearly indicates a mixture of isomers and has diagnostic bands for both enol/amino (**1** and **2**) and keto/amino species (**3** and **4**) as discussed below. A linear combination (LC) of the four isomers was considered and displayed a suitable match for the experimental spectra (see *LC 1-4* in Figure 2).

This situation is similar to that of the protonated cytosine previously studied by Maître, Salpin, and co-workers via IRMPD action spectroscopy.[10] The two lowest energy isomers of [Cyt+H]$^+$, shown as species **B** and **C** (Scheme 1), within 0.3 kJ

Table 1. Experimental and theoretical vibrational frequencies for the cytosine radical cation.

Exp.[a]	Theoretical cytosine radical cation				Vibrational modes[c]
	1[b]	2[b]	3[b]	4[b]	
1650 (0.68)	1632 (98)	1630 (65)	1645 (494)	1667 (218)	$\delta_s NH_2$
				1641 (133)	$\nu C{=}O + \delta_s NH_2$
1560 (0.87)		1561 (380)			$\nu_{as}N_3C_2O + \delta_s NH_2 + \delta OH$
			1576 (132)		$\nu C_5C_6 + \delta_s NH_2$, highly coupled
1525 (0.94)	1526 (253)				$\nu_{as}N_3C_2O + \delta_{as}NH_2 + \delta OH$
	1516 (404)				$\nu N_3C_4 + \nu C_2O + \nu N1C6$
		1516 (128)			$\nu N_3C_4 + \delta_{as}NH_2 + \nu N1C6$
1505 (1.0)	1491 (71)	1485 (39)			$\nu_{as}N_8C_4C_5 + \delta C_5H$
			1486 (91)		$\delta N_1H + \nu C_4N_8 + \delta_s NH_2$
				1491 (94)	νC_4C_5, highly coupled
1415 (0.72)	1429 (72)	1410 (397)			$\nu N_1C_2 + \delta OH + \delta C_6H$
				1403 (34)	$\nu C_5C_6 + \delta C_6H$
1380 (0.67)	1367 (72)	1367 (59)			δC_6H, highly coupled
			1365 (63)		νN_3C_4, highly coupled
1240 (0.30)	1218 (160)	1220 (110)			δOH
			1231 (42)		$\delta N_1H + \rho NH_2 + \delta C_5H + \delta C_6H$
1100 (0.28)			1152 (134)		$\rho NH_2 + \nu N_1C_6 + \nu C{=}O + \delta N_1H + \delta C_6H$
				1116 (66)	$\nu_{as}N_1C_2N_3 + \nu C_5C_6 + \delta C_5H + \delta C_6H$
				1082 (47)	$\rho NH_2 + \nu C_2N_3 + \delta C_5H$

[a] Experimental frequency in cm^{-1} (relative intensity in parenthesis). [b] Theoretical frequency in cm^{-1} (km mol^{-1} intensity in parenthesis). Scaled by a factor of 0.98. [c] See numbering system in Scheme 1.

mol^{-1} of one another, were found to be potentially contributing to the experimentally observed IRMPD spectrum in the fingerprint region. Additional isomers were calculated to be much higher in energy and did not match the experimental IR spectrum.[11b]

Analysis of the individual absorbance bands and the corresponding theoretically predicted vibrational modes (Table 1) reveals that each isomer contributes substantially to the observed experimental spectrum. The peak at ~ 1650 cm^{-1} correlates primarily to the strong absorbance from the scissoring motion of the NH_2 group ($\delta_s NH_2$) which was most intense in the keto/amino forms **3** and **4**. Combined carbonyl stretching motion ($\nu C{=}O$) and NH_2 scissoring was found with a relatively high intensity in **4**, also contributing to the 1650 cm^{-1} peak. The enol/amino species **1** and **2** have less intense $\delta_s NH_2$ modes that are slightly red-shifted from their keto/amino counterparts and may cause the peak shoulder observed at ~1630 cm^{-1}. A sharp peak at ~1560 cm^{-1} in the IRMPD spectrum may result from the coupled asymmetric stretching of the C_2-N_3-O ($\nu_{as}N_3C_2O$), the asymmetric NH_2 scissoring ($\delta_s NH_2$), and the OH bending (δOH) vibrational mode calculated to be an intense mode of species **2**. Assigning the split peaks at ~1505 cm^{-1} and ~1525 cm^{-1} is challenging. However, species **1** has two strong vibrational modes in this range at 1526 cm^{-1} (the analogous mode to that found in species **2** at ~1560 cm^{-1}) and 1516 cm^{-1}, which is the most intense mode from the coupled N_3-C_4 (νN_3C_4), C_2-OH (νC_2O), and N_1C_6 (νN1C6) stretching. Species **2** possess a similar mode at 1516 cm^{-1} that likely also contributes to the large observed peak in this region. All four of the low energy structures calculated have less intense and highly-coupled vibrational modes in the 1485-1500 cm^{-1} region, likely resulting in the broadening and tailing of the larger peak towards the lower frequencies. The observed peak at 1415 cm^{-1} aligns well with the intense mode calculated for species **2** for the N_1-C_2 (νN_1C_2) stretch coupled with the OH (δOH) and C_6H (δC_6H) bending motions. An analogous vibrational mode is also present although less intense, in species **1**. The neighboring peak at ~1380 cm^{-1} is closely approximated by the highly coupled δC_6H motion of species **1** & **2** at 1367 cm^{-1} and the νN_3C_4 mode in species **3** at 1365 cm^{-1}. In the lower-frequency region of the experimental spectrum, several low intensity peaks are observed and correspond to highly coupled vibrational modes. Notably, the O-H bending motion in the enol/amino species **1** and **2** is calculated to be reasonably intense at ~1220 cm^{-1}, possibly contributing substantially to the broad experimental peak found at ~1240 cm^{-1}. The final peak near 1100 cm^{-1} is matched most reasonably by two vibrational modes calculated for species **4** (at 1116 cm^{-1} and 1082 cm^{-1}) which bracket the experimentally observed peak.

Gas-phase action spectroscopy – UV-PD

Single-photon UV-PD action spectroscopy was also acquired for the cytosine (M) radical cation generated from the $[Cu^{II}(terpy)(M)]^{\bullet 2+}$ complex. The experimental UV-PD spectra in the 210 – 700 nm range for the cytosine radical cations were generated from the combination of two fragmentation channels: the loss of 28 and 42 Da (Figure 3). These fragments were consistently seen in both IRMPD and CID experiments and are assigned to the neutral losses of CO and NCO. Such eliminations were found previously and explored theoretically.[17g] As the barrier toward such eliminations was found higher in energy than the transition states leading to isomerization of the cytosine radical cation,[17g] the fragments cannot be diagnostic in the determination of the species present in the gas phase. The action spectrum showed several bands that were represented by the neutral losses mentioned above. Weak bands were observed at 600, 530, and 455 nm, whereas stronger bands appeared at 400, 350, 280 (shoulder), and 260 nm. The short

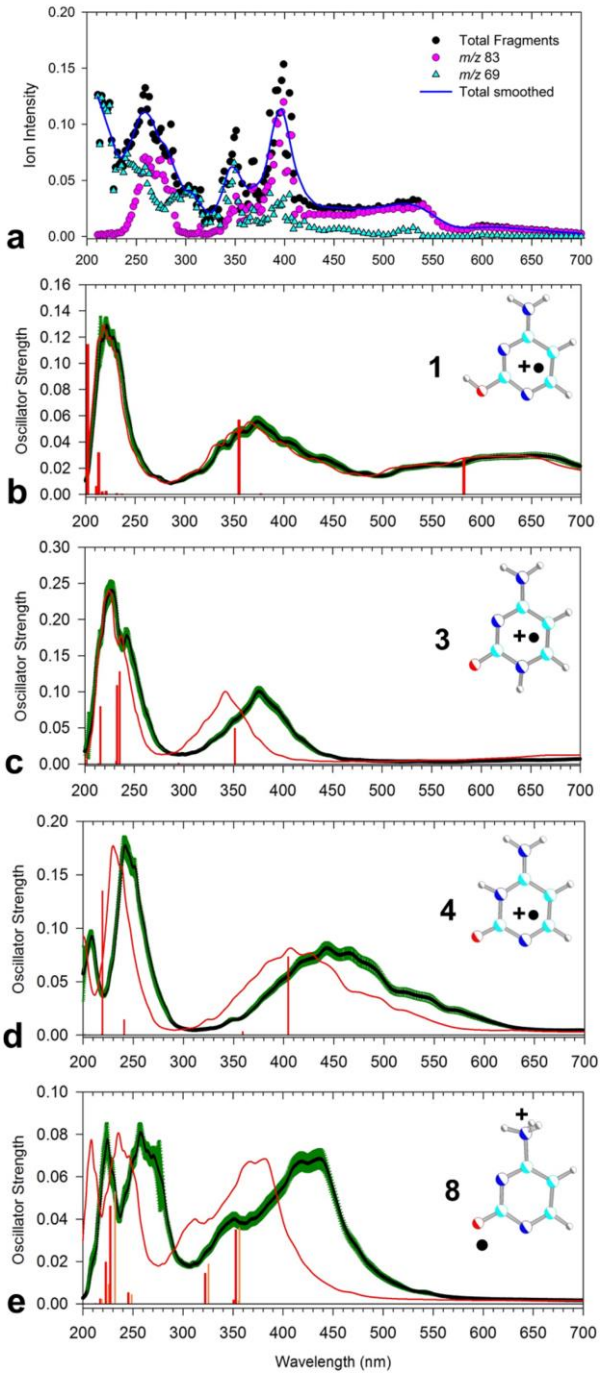

Figure 3. (a) Experimental UV-PD action spectra of the cytosine radical cation displaying individual fragmentation channels, total fragments, and the smoothed pattern as indicated in the legend. The spectrum is compiled from the average of two individual runs on separate days. Calculated TD-DFT M06-2X/6-311++G(2d,p) (black lines) of (b) **1**, (c) **3**, (d) **4**, and (e) **8**. The green error bars are from Newton-X calculations of vibronic transitions at 300 K. Red bars represent the EOM-CCSD/6-31+G(d,p) absorption lines. The red curves depict wavelength-benchmarked vibronic spectra based on a linear correlation of M06-2X and EOM-CCSD calculated transition energies.

wavelength band at <210 nm appeared only in the m/z 69 (loss of NCO) channel. The action spectrum of cytosine cation radical substantially differs from the UV spectrum of neutral cytosine which shows the longest wavelength absorption maximum at 270 nm.[24]

Interestingly, none of the four low-energy isomers of the cytosine radical cation had the same calculated absorption band pattern as that found in the experimental UV-PD spectrum (Figure 3a, see Figure S4 for additional theoretical spectra). The long wavelength band at 600 nm is represented by an absorption band in the spectrum of **1** (Figure 3b) whereas the 530 and 455 nm bands appear in **1** and **4** (Figure 3d). The 350 nm band appears in **1** and **3** (Figure 3c) whereas the 400 nm band appears in **4**. Isomer **2** UV-PD spectrum (Figure S4) is very similar to that of **1**. All these isomers also show strong absorption bands at 230-260 nm approximately matching the 260 nm experimental band. Thus, concurring with the IRMPD data, the UV-PD action spectra indicate the presence of several cytosine cation radical isomers that are formed by intramolecular electron transfer in the gas-phase $[Cu^{II}(terpy)(M)]^{\bullet 2+}$ complex. Interestingly, a reasonable match to the 250-450 nm region of the action spectrum was found for the calculated absorption spectrum of the high-energy isomer **8** (Figure 3e). This feature, not revealed by IRMPD, does not rule out the potential presence of the formally distonic radical cation (with the charge at the amine and the unpaired spin on the oxygen atom, species **8**). However, this ion is more than 120 kJ mol^{-1} higher in energy than the keto/amino and enol/amino tautomers (Figure 1 and Table S1), and so its formation appears unlikely and is discussed further below.

Comparison of UV and IR spectroscopy results

Given that both IR and UV action spectroscopy data point to a mixture of several $Cyt^{\bullet +}$ isomers present in the gas phase during laser activation, their origin needs to be discussed. As the radical cation of cytosine is formed via CID of the $[Cu^{II}(terpy)(M)]^{\bullet 2+}$ complex, the structure of this complex, both in solution and in the gas phase, may affect the structure of the resulting $Cyt^{\bullet +}$ ions. The relative energies of selected $[Cu^{II}(terpy)(M)]^{\bullet 2+}$ complexes were obtained for fully optimized structures (Figure S5), corresponding to ligation of Cu(terpy) by different cytosine tautomers (we considered two binding modes of **1**, and one each for **4** and **8**). Consistent with the order of relative energies for $Cyt^{\bullet +}$, the N1-ligated $[Cu(terpy)(\mathbf{4}\text{-N1})]^{\bullet 2+}$ complex was found to be lowest in energy, closely followed by the isomer **1** also bound via N1. Since the complexes are formed in solution, solvation effects were considered by running Polarizable Continuum Model[25] calculations in water and methanol. Although there are some energy differences between the complexes due to different solvation, the relative differences between isomers **4** and **1** bound to Cu(terpy) in solution are still minor. Therefore, it is reasonable to suggest that the mixture of $Cyt^{\bullet +}$ isomers results from the isomeric Cu complexes found in solution.

Formation of the $Cyt^{\bullet +}$ isomeric mixture is also possible during CID of the $[Cu^{II}(terpy)(M)]^{\bullet 2+}$ complexes when $Cyt^{\bullet +}$ ions

dissociating from the complex carry excess energy sufficient for isomerization. It has previously been established computationally by Wolken *et al*. that isomerization between the low energy isomers of cytosine radical cation would take less energy than their fragmentation.[17g] The most energetically favorable elimination channel (loss of CO) was found to have a critical transition state energy of 180 kJ mol^{-1}, relative to the lowest energy isomer (**4**), at the CCSD(T)/6-311++G(3df,2p) level of theory.[17g] Isomerization pathways of species **1**-**4**, were found to proceed through transition states with energies of 145 - 174 kJ mol^{-1} relative to ion **4** at the same level of theory.[17g] Therefore, is not inconceivable that the radical cation of cytosine formed during the CID of the Cu complex will be able to rearrange before the spectroscopy experiments. This would result in a mixture of low energy isomers as the best match to the experimental IRMPD and UV-PD spectroscopy data.

We investigated the possibility that the distonic ion (**8**) was co-formed via dissociation of the copper complex (Eq. 1, where M = Cyt, and Scheme S1). The properties of this highly energetic isomer and its ability to rearrange into more stable species is discussed in detail in the supporting information (Discussion of isomer **8**, Schemes S2-S3, Figures S6-S7). However, the O-ligated [Cu(terpy)(**8**-O)]$^{\bullet 2+}$ complex was found higher in energy than the **4** counterpart by 97 kJ mol^{-1} and higher than the other isomers in the gas phase (Figure S5 and Table S3). Although the energy differences between the complexes somewhat decreased due to different solvation, complex [Cu(terpy)(**8**-O)]$^{\bullet 2+}$ was still >90 kJ mol^{-1} less stable than [Cu(terpy)(**4**-N1)]$^{\bullet 2+}$ and also substantially less stable than the other solvated complexes in both water and methanol. Thus, is seems unlikely that [Cu(terpy)(**8**-O)]$^{\bullet 2+}$ was present under equilibrium conditions in bulk solution.

Ion-molecule reactions (IMR)

The gas-phase reactivity of the cytosine radical cation (Cyt$^{\bullet +}$) was explored toward a variety of neutral reagents including nitric oxide, dimethyl disulfide, and *n*-propyl thiol. This resulted in the following reactivity (where M = Cyt):

Radical recombination: $M^{\bullet +} + {}^{\bullet}NO \rightarrow M\text{-}NO^{+}$ (Eq. 2)
Electron transfer: $M^{\bullet +} + CH_3SSCH_3 \rightarrow M + CH_3SSCH_3^{\bullet +}$ (Eq. 3)
Hydrogen abstraction: $M^{\bullet +} + RSH \rightarrow MH^{+} + RS^{\bullet}$ (Eq. 4)

The corresponding mass spectra are given in Figure S8.

Exposing Cyt$^{\bullet +}$ to nitric oxide produced the $^{\bullet}$NO addition reaction (Eq. 2) characteristic of σ-radicals.[26] It is notable that this reaction can potentially occur at both the N- and O-based radical locations in cytosine radical cation. In the enol/amino structures (**1** and **2**) there is a substantial spin density (0.33) at N1 atom and only minimal unpaired spin at the hydroxyl O7. The keto/amino structures (**3** and **4**) possess significant spin density at the carbonyl O7 (0.49 and 0.27, respectively), as well as considerable spin density at the unprotonated N (0.29 at N3 and 0.40 at N1, respectively). We have previously shown that highly delocalized phenoxy radicals display reactivity towards nitric oxide even when the spin density at the oxygen atom is as low as 0.17.[27]

Electron transfer reaction (Eq. 3) dominated the reactivity with dimethyl disulfide (IP ≅ 8.2 eV[28]), as demonstrated by the appearance of the charged product at *m/z* 94. Such reactions often occur when a more stable radical ion can be formed (of the two neutral species in Eq. 3, the one with the lower IP will become the cation). We found such reactions typical for a highly delocalized π-radical of tryptophan.[26] For Cyt$^{\bullet +}$, the ionization energies were calculated previously to be in the range of 8.2 – 8.9 eV depending on the specific tautomer and level of theory,[17g] in agreement with the experimental values[29] that have recently been narrowed to 8.695-8.738 eV.[29]

The hydrogen abstraction reaction was found to be the main process for the cytosine radical cation in the presence of *n*-propyl thiol (Eq. 4). This reaction leads to the protonated cytosine and can also occur via the O- or N-based radical site. In effect, that will result in a new O-H or N-H bond and a thiyl radical (RS$^{\bullet}$). This type of hydrogen atom abstraction was theoretically predicted by Tehrani *et al.* as a typical reaction for the cytosine radical cation.[30] They calculated the reaction to be exothermic by ~75 kJ mol^{-1} and noted that only a small activation barrier was required.[30]

While this reactivity cannot be used to discern the isomeric composition of Cyt$^{\bullet +}$, it is consistent with the reactivity trends predicted for nucleobase radicals. These trends suggest that if an electron is stripped from the Cyt site, resulting in a transient radical cation species, a facile hydrogen atom or electron transfer reaction may follow. This will lead to propagation of the radical site either intramolecularly within the DNA chain or intermolecularly through reactions with neighboring species.

Conclusions

This combined experimental and computational study allows us to arrive at the following conclusions. Cytosine radical cations are formed as a mixture of isomers upon collision-induced oxidation of the cytosine ligand via dissociation from the copper (II) ternary complex, [Cu^{II}(terpy)(M)]$^{\bullet 2+}$. A mixture of several low-energy isomers was also found in a recent investigation of cytosine radical cations formed via VUV photodissociation.[18] This is consistent with the existence of multiple Cyt$^{\bullet +}$ isomers within 10 kJ mol^{-1} of one another as found by multiple level of theory. In this work, the Cyt$^{\bullet +}$ isomeric mixture may originate from different [Cu^{II}(terpy)(M)]$^{\bullet 2+}$ isomers present in solution or from the gas-phase rearrangement of Cyt$^{\bullet +}$ upon CID of the Cu complex. IRMPD action spectroscopy points to a mixture of low energy amino-type Cyt$^{\bullet +}$ tautomers (**1**-**4**) that contribute to the vibrational signature in the fingerprint region. The UVPD action spectroscopy spectrum similarly contains features of the low energy Cyt$^{\bullet +}$ ions. The presence of a high-energy distonic isomer **8** which displayed a reasonable UV-PD match was considered. Analysis of energy data for gas-phase Cyt$^{\bullet +}$ and [Cu^{II}(terpy)(M)]$^{\bullet 2+}$ complexes in solution and the gas phase indicates that the formation of isomer **8** is unlikely. As all isomers possess highly delocalized unpaired spin, ion-molecule

reactions are unable to shed light on the isomeric composition of the Cyt radical cation population. They do, however, reveal that the cytosine radical cations are highly reactive and undergo facile hydrogen atom tranfer, electron transfer, and radical recombination reactions.

Experimental Section

Materials. All chemicals and reagents were used as received without any additional purification. Cytosine, copper(II) nitrate trihydrate, 2,2':6',2"-terpyridine, *n*-propyl thiol, and dimethyl disulfide were purchased from Sigma-Aldrich (Milwaukee, WI). Methanol (HPLC grade) was purchased from Fisher Scientific (Pittsburg, PA). Premixed gas containing 1% nitric oxide in laser grade helium was purchased from Airgas (Chicago, IL). Water was purified (18 MΩ) in house.

Sample preparation. Stock solutions (1 mg/mL) of cytosine, and 2,2':6',2"-terpyridine (terpy) were each prepared in methanol, and $Cu(NO_3)_2$ (1 mg/mL) was prepared in 50:50 methanol/water. The stock solutions of terpy and $Cu(NO_3)_2$ were combined 1:1 and diluted 10-fold in methanol. An aliquot of this solution was then combined 1:1 with the stock solution cytosine, vortexed and allowed to react for 10 min. at room temperature. The resulting mixture was diluted with methanol to an appropriate concentration for direct infusion into the mass spectrometer. Cytosine radical generation was accomplished via successive isolation of the ternary metal complex, $[Cu^{II}(terpy)(M)]^{2+}$, where M= cytosine, CID of the complex, and isolation of the dissociation product $M^{\bullet+}$.

Ion-molecule reactions. The isolated radical cations were subjected to IMRs with the neutral species nitric oxide, *n*-propyl thiol, and dimethyl disulfide via a modified Bruker Esquire 3000 quadrupole ion trap mass spectrometer (Bruker Daltronics, Bremen, Germany), as previously described.[31] Reactions with nitric oxide were achieved by introducing nitric oxide into the trap via the helium line from a 1% nitric oxide in helium premixed cylinder. The internal helium regulator was unmodified from normal usage. The dimethyl disulfide and *n*-propyl thiol were introduced to the trap through a leak valve. In all cases, a scan delay of 500 ms was employed as the reaction time.

IRMPD action spectroscopy. Gas-phase infrared spectra of the cytosine radical cation were acquired using the FEL beamline at the Centre Laser Infrarouge d'Orsay (CLIO) facility. Solutions were prepared as previously described. Radical formation was achieved by using CID in the modified ion trap of the Bruker Esquire 3000+ (Bruker Daltonics, Bremen, Germany) quadrupole ion trap mass spectrometer, and were subsequently mass selected. Details of the instrumental setup are described elsewhere.[32] IRMPD was performed on the mass-selected ions, and mass spectra were recorded over eight averages with a wavenumber step of 4.5 cm^{-1}, an irradiation time of 1 s, and laser power of 700-1500 mW. To ensure reproducibility, each spectrum was acquired twice. The IRMPD spectra were produced based on -ln (fragment ion/fragment+parent ion) signal ratio as a function of excitation wavenumber.

UV-PD action spectroscopy. Tandem MS (i.e. UVPD-MS^n and CID-MS^n) and action spectroscopy were performed on an LTQ-XL-ETD linear ion trap (ThermoElectron Fisher, San Jose, CA) modified with an external EKSPLA NL301G (Altos Photonics, Bozeman, MT, USA) Nd-YAG laser source operating at 20 Hz frequency with a 3-6 ns pulse width.[33] The pump laser is interfaced to the LTQ via LabView software (National Instruments, Austin, TX, USA), and generates photons which are directed into a PG142C unit (Altos Photonics, Bozeman, MT, USA). The PG142C unit consists of a third harmonic generator and optical parametric oscillator coupled with an optional second harmonic generator (SH), and provides wavelength tuning between 210-700 nm at 0.52-12.69 mJ/pulse peak. The power of the PG142C output beam was measured at each wavelength using an EnergyMax-USB J-10MB energy sensor (Coherent Inc., Santa Clara, CA, USA). After recording the power readings, the energy sensor was removed from the beam path, and the PG142C output beam (6-mm diameter) was focused through a small aperture drilled in the CI source and into the linear ion trap. In this particular case, the typical experimental setup consisted of electro-spraying our copper ternary complex solution into the ion trap, performing CID on the doubly-charged complex to produce the desired singly-charged nucleobase cation radical, and then isolating the nucleobase cation radical for photo-activation from 210-700 nm. The intensities of the resulting UVPD-MS^3 photo-fragments were monitored as a function of wavelength, and their final intensities were normalized to the laser output power to plot the action spectra. The number of laser pulses used during each isolation depended on the degree of photo-dissociation at each given wavelength, and ranged from 1 to 19 pulses (i.e. 100 to 1000 ms activation time, respectively, with each successive pulse spaced by 50 ms).

More specifically, the prepared cytosine-copper ternary complex solution was introduced into the ESI source of the mass spectrometer at a flow rate of 1 uL/min in the positive ion mode. The spray voltage, capillary temperature, and capillary voltage were adjusted to 2.7 kV, 275 °C, and 15 V, respectively. The doubly-charged cytosine-copper ternary complex (*m/z* 203.5) was isolated using a 2 *m/z* isolation window and subjected to CID at 35 NCE for 30 ms. The resulting singly-charged cytosine cation radical (*m/z* 111) produced via oxidative dissociation from the ternary complex was then isolated with a 5 *m/z* isolation window and subjected to action spectroscopy via UVPD. The number of laser pulses used throughout the SSH/FSH (210-354 nm), ESH (355-409 nm), and PG region (410-700 nm) ranged from 3, 15, and 1 pulse(s), respectively (i.e. 200, 750, and 100 ms activation times). "Blank" background scans were also recorded to avoid "false" photo-fragment peak assignments due to spectral noise produced by the laser.

Calculations. All calculations were performed using the Gaussian 09 quantum chemical program.[34] Geometries were optimized within the framework of Becke's three-parameter DFT hybrid functional (B3LYP) and the 6-311++G(d,p) basis set. All optimized structures were subjected to vibrational frequency analyses to ensure that they corresponded to minima (no imaginary frequencies) and transition states (1 imaginary frequency). For comparison of theoretical IR absorbance bands and the experimental IRMPD spectroscopy, a scaling factor of 0.98 was applied to the predicted IR spectra as calculated at the B3LYP/6311++G(d,p) level. This scaling factor is known to be appropriate for DFT comparison with IRMPD spectra.[35] Predicted IR peaks were convoluted using Gaussian profiles with a full width at half-maximum of 30 cm^{-1}.

Another set of optimized geometries and relative energies of all cytosine cation-radical tautomers were obtained with the ωB97X-D[36] and M06-2X[37] hybrid functionals using the 6-311+G(2d,p) basis set. At our highest level of theory, select structures were optimized with UMP2(full)/6-31G(d,p) and used for single-point energy coupled-cluster calculations[38] with single, double, and disconnected triple excitations,[39] CCSD(T), with the aug-cc-pVTZ basis set,[40] providing benchmark relative energies. All these calculations were performed for doublet spin states within the spin-unrestricted formalism. Vertical excitation energies and transition intensities (oscillator strengths) were calculated for lowest 25 excited states with time-dependent DFT calculations[41] using the ωB97X-D and M06-2X functionals and the 6-311+G(2d,p) basis set. Another set of excitation energies were obtained with equation-of-motion

calculations with coupled clusters and single and double excitations (EOM-CCSD)[42] using the 6-31+G(d,p) basis set and, for structures **4** and **8** also using the 6-311+G(2d,p) basis set, to benchmark the TD-DFT energies.[43] The EOM-CCSD/6-31+G(d,p) and 6-311+G(2d,p) calculations of **4** and **8** showed nearly identical results (Table S2, Supporting Information) with root mean square deviations of absorption wavelentgths of rmsd < 2.3 nm. The smaller 6-31+G(d,p) basis set was then used in EOM-CCSD calculations of all cytosine cation radicals. Comparison of the TD-DFT and EOM-CCSD data showed a closer agreement between the M06-2X and EOM-CCSD benchmark computations for most of the cytosine structures (Table S2, Supporting Information), and this functional was therefore used to further compute the vibronically-broadened absorption spectra at 300 K.[44]

Vibronically-broadened spectra were generated with Newton-X (version 1.4, www.newtonx.org),[45] PuTTY 0.67 SSH suite (Simon Tatham, 1997-2016), Xming (Colin Harrison, 2005-2007), and WinSCP (Martin Prikryl, 2000-2016) programs. Optimized Cartesian atomic coordinates and harmonic frequencies obtained with M06-2X/6-31+G(d,p) were used to generate random configurations that were weighted according to their Boltzmann factors at 300 K. A total of 12 excited electronic states and 500 configurations were used to produce each spectrum.

Acknowledgements

This study was supported by Northern Illinois University. M.L. thanks the Graduate School of NIU for the Dissertation Completion Fellowship. F.T. thanks the Chemistry Division of the National Science Foundation for funding (Grants CHE-1359810 and CHE-1543805).

Keywords: nucleobases • radical ions • UV-PD spectroscopy • IRMPD spectroscopy • ion-molecule reactions

[1] a) R. P. Rastogi, A. Kumar, M. B. Tyagi, R. P. Sinha, *J. Nucleic Acids* **2010**, *2010*; b) A. Kumar, M. D. Sevilla, *Chem. Rev.* **2010**, *110*, 7002-7023.

[2] a) J. Cadet, T. Douki, J.-L. Ravanat, *Free Radical Biol. Med.* **2010**, *49*, 9-21; b) C. J. Burrows, J. G. Muller, *Chem. Rev.* **1998**, *98*, 1109-1152.

[3] W. A. Glass, M. N. Varma, *Physical and chemical mechanisms in molecular radiation biology, Vol. 58*, Springer Science & Business Media, **2012**.

[4] S. Steenken, *Chem. Rev.* **1989**, *89*, 503-520.

[5] a) F. Greco, A. Liguori, G. Sindona, N. Uccella, *J. Am. Chem. Soc.* **1990**, *112*, 9092-9096; b) A. Liguori, A. Napoli, G. Sindona, R. Cooks, *Rapid Commun. Mass Spectrom.* **1994**, *8*, 89-93.

[6] M. Rodgers, P. B. Armentrout, *J. Am. Chem. Soc.* **2000**, *122*, 8548-8558.

[7] J. Gidden, J. E. Bushnell, M. T. Bowers, *J. Am. Chem. Soc.* **2001**, *123*, 5610-5611.

[8] J. Gidden, M. T. Bowers, *Eur. Phys. J. D* **2002**, *20*, 409-419.

[9] a) D. Liu, T. Wyttenbach, M. T. Bowers, *J. Am. Chem. Soc.* **2006**, *128*, 15155-15163; b) J. Gidden, M. T. Bowers, *J. Phys. Chem. B* **2003**, *107*, 12829-12837.

[10] J. Y. Salpin, S. Guillaumont, J. Tortajada, L. MacAleese, J. Lemaire, P. Maitre, *ChemPhysChem* **2007**, *8*, 2235-2244.

[11] a) J. M. Bakker, R. K. Sinha, T. Besson, M. Brugnara, P. Tosi, J.-Y. Salpin, P. Maître, *J. Phys. Chem. A* **2008**, *112*, 12393-12400; b) J. M. Bakker, J.-Y. Salpin, P. Maître, *Int. J. Mass Spectrom.* **2009**, *283*, 214-221.

[12] a) J. Y. Salpin, D. Scuderi, *Rapid Commun. Mass Spectrom.* **2015**, *29*, 1898-1904; b) A. Filippi, C. Fraschetti, F. Rondino, S. Piccirillo, V. Steinmetz, L. Guidoni, M. Speranza, *Int. J. Mass Spectrom.* **2013**, *354*, 54-61; c) R. Wu, B. Yang, C. Frieler, G. Berden, J. Oomens, M. Rodgers, *Phys. Chem. Chem. Phys.* **2015**, *17*, 25978-25988; d) R. Wu, B. Yang, C. Frieler, G. Berden, J. Oomens, M. Rodgers, *J. Phys. Chem. B* **2015**, *119*, 5773-5784.

[13] Y. w. Nei, K. T. Crampton, G. Berden, J. Oomens, M. T. Rodgers, *J. Phys. Chem. A* **2013**, *117*, 10634-10649.

[14] B. Yang, R. R. Wu, G. Berden, J. Oomens, M. T. Rodgers, *J. Phys. Chem. B* **2013**, *117*, 14191-14201.

[15] a) B. Yang, R. Wu, N. Polfer, G. Berden, J. Oomens, M. Rodgers, *J. Am. Soc. Mass Spectrom.* **2013**, *24*, 1523-1533; b) E. A. Gillis, K. Rajabi, T. D. Fridgen, *J. Phys. Chem. A* **2008**, *113*, 824-832; c) E. A. Gillis, T. D. Fridgen, *Int. J. Mass Spectrom.* **2010**, *297*, 2-8; d) K. Rajabi, E. A. Gillis, T. D. Fridgen, *J. Phys. Chem. A* **2010**, *114*, 3449-3456.

[16] a) J. M. Rice, G. O. Dudek, M. Barber, *J. Am. Chem. Soc.* **1965**, *87*, 4569-4576; b) J. M. Rice, G. O. Dudek, *J. Am. Chem. Soc.* **1967**, *89*, 2719-2725.

[17] a) F. Tureček, *J. Mass Spectrom.* **1998**, *33*, 779-795; b) J. K. Wolken, F. Turecek, *J. Phys. Chem. A* **1999**, *103*, 6268-6281; c) J. K. Wolken, F. Tureček, *J. Phys. Chem. A* **2001**, *105*, 8352-8360; d) X. Chen, E. A. Syrstad, M. T. Nguyen, P. Gerbaux, F. Tureček, *J. Phys. Chem. A* **2005**, *109*, 8121-8132; e) C. Yao, M. L. Cuadrado-Peinado, M. Polášek, F. Tureček, *Angew. Chem. Int. Ed* **2005**, *44*, 6708-6711; f) F. Tureček, *Adv. Quantum Chem.* **2007**, *52*, 89-120; g) J. K. Wolken, C. Yao, F. Tureček, M. J. Polce, C. Wesdemiotis, *Int. J. Mass Spectrom.* **2007**, *267*, 30-42.

[18] Z. Chen, K.-C. Lau, G. A. Garcia, L. Nahon, D. K. Božanić, L. Poisson, M. M. Al-Mogren, M. Schwell, J. S. Francisco, A. Bellili, M Hochlaf, *J. Am. Chem. Soc.* **2016**, *138*, 16596-16599.

[19] a) I. K. Chu, C. F. Rodriquez, T.-C. Lau, A. C. Hopkinson, K. W. M. Siu, *J. Phys. Chem. B* **2000**, *104*, 3393-3397; b) I. K. Chu, C. F. Rodriguez, A. C. Hopkinson, K. W. M. Siu, T.-C. Lau, *J. Am. Soc. Mass Spectrom.* **2001**, *12*, 1114-1119; c) E. Bagheri-Majdi, Y. Ke, G. Orlova, I. K. Chu, A. C. Hopkinson, K. W. M. Siu, *J. Phys. Chem B* **2004**, *108*, 11170-11181.

[20] a) S. Wee, R. A. J. O'Hair, W. D. McFadyen, *Rapid Commun. Mass Spectrom.* **2005**, *19*, 1797-1805; b) A. K. Lam, B. F. Abrahams, M. J. Grannas, W. D. McFadyen, R. A. J. O'Hair, *Dalt. Trans.* **2006**, 5051-5061.

[21] L. Feketeová, G. N. Khairallah, B. Chan, V. Steinmetz, P. Maître, L. Radom, R. A. J. O'Hair, *Chem. Comm.* **2013**, *49*, 7343-7345.

[22] L. Feketeová, B. Chan, G. N. Khairallah, V. Steinmetz, P. Maître, L. Radom, A. Richard, *Phys. Chem. Chem. Phys.* **2015**, *17*, 25837-25844.

[23] S. Ø. Pedersen, C. S. Byskov, F. Turecek, S. B. Nielsen, *J. Phys. Chem. A* **2014**, *118*, 4256-4265.

[24] a) F. Zaloudek, J. S. Novros, L. B. Clark, *J. Am. Chem. Soc.* **1985**, *107*, 7344-7351; b) H. Du, R. C. A. Fuh, J. Li, L. A. Corkan, J. S. Lindsey, *Photochem. Photobiol.* **1998**, *68*, 141-142; c) C. T. Middleton, K. de La Harpe, C. Su, Y. K. Law, C. E. Crespo-Hernández, B. Kohler, *Annu. Rev. Phys. Chem.* **2009**, *60*, 217-239

[25] J. Tomasi, B. Mennucci, R. Cammi, *Chem. Rev.* **2005**, *105*, 2999-3094.

[26] A. Piatkivskyi, S. Osburn, K. Jaderberg, J. Grzetic, J. D. Steill, J. Oomens, J. Zhao, J. K.-C. Lau, U. H. Verkerk, A. C. Hopkinson, V. Ryzhov, *J. Am. Soc. Mass Spectrom.* **2013**, *24*, 513-523.

[27] M. Lesslie, A. Piatkivskyi, J. Lawler, T. R. Helgren, S. Osburn, R. A. J. O'Hair, V. Ryzhov, *Int. J. Mass Spectrom.* **2015**, *390*, 124-131.

[28] D. T. Leeck, H. I. Kenttämaa, *Org. Mass. Spectrom.* **1994**, *29*, 106-107.

[29] a) D. Dougherty, E. Younathan, R. Voll, S. Abdulnur, S. McGlynn, *J. Electron. Spectrosc. Relat. Phenom.* **1978**, *13*, 379-393; b) N. Hush, A. S. Cheung, *Chem. Phys. Lett.* **1975**, *34*, 11-13.

[30] Z. A. Tehrani, M. J. Javan, A. Fattahi, M. M. Hashemi, *J. Theor. Comput. Chem.* **2012**, *11*, 313-327.

[31] Y. Pyatkivskyy, V. Ryzhov, *Rapid Commun. Mass Spectrom.* **2008**, *22*, 1288-1294.

[32] L. Mac Aleese, A. Simon, T. B. McMahon, J.-M. Ortega, D. Scuderi, J. Lemaire, P. Maître, *Int. J. Mass Spectrom.* **2006**, *249*, 14-20.

[33] a) C. J. Shaffer, R. Pepin, F. Tureček, *J. Mass Spectrom.* **2015**, *50*, 1438-1442; b) H. T. Nguyen, C. J. Shaffer, R. Pepin, F. Tureček, *J. Phys. Chem. Lett.* **2015**, *6*, 4722-4727; c) E. Viglino, C. J. Shaffer, F. Tureček, *Angew. Chem. Int. Ed.* **2016**.

[34] M. J. Frisch, G. W. Trucks, H. B. Schlegel, G. E. Scuseria, M. A. Robb, J. R. Cheeseman, G. Scalmani, V. Barone, B. Mennucci, G. A. Petersson, H. Nakatsuji, M. Caricato, X. Li, H. P. Hratchian, A. F. Izmaylov, J. Bloino, G. Zheng, J. L. Sonnenberg, M. Hada, M. Ehara, K. Toyota, R. Fukuda, J. Hasegawa, M. Ishida, T. Nakajima, Y. Honda, O. Kitao, H. Nakai, T. Vreven, J. A. Montgomery Jr., J. E. Peralta, F. Ogliaro, M. J. Bearpark, J. Heyd, E. N. Brothers, K. N. Kudin, V. N. Staroverov, R. Kobayashi, J. Normand, K. Raghavachari, A. P. Rendell, J. C. Burant, S. S. Iyengar, J. Tomasi, M. Cossi, N. Rega, N. J. Millam, M. Klene, J. E. Knox, J. B. Cross, V. Bakken, C. Adamo, J. Jaramillo, R. Gomperts, R. E. Stratmann,

O. Yazyev, A. J. Austin, R. Cammi, C. Pomelli, J. W. Ochterski, R. L. Martin, K. Morokuma, V. G. Zakrzewski, G. A. Voth, P. Salvador, J. J. Dannenberg, S. Dapprich, A. D. Daniels, Ö. Farkas, J. B. Foresman, J. V. Ortiz, J. Cioslowski, D. J. Fox, Gaussian, Inc., Wallingford, CT, USA, **2009**.

[35] a) J. Steill, J. Zhao, C. K. Siu, Y. Ke, U. H. Verkerk, J. Oomens, R. C. Dunbar, A. C. Hopkinson, K. W. M. Siu, *Angew. Chem.* **2008**, *120*, 9812-9814; b) J. Zhao, J. K.-C. Lau, J. Grzetic, U. H. Verkerk, J. Oomens, K. W. M. Siu, A. C. Hopkinson, *J. Am. Soc. Mass. Spectrom.* **2013**, *24*, 1957-1968; c) O. Hernandez, B. Paizs, P. Maître, *Int. J. Mass Spectrom.* **2015**, *377*, 172-178.

[36] J.-D. Chai, M. Head-Gordon, *Phys. Chem. Chem. Phys.* **2008**, *10*, 6615-6620.

[37] Y. Zhao, D. G. Truhlar, *Theor. Chem. Acc.* **2008**, *120*, 215-241.

[38] J. Čížek, J. Paldus, L. Šroubková, *Int. J. Quantum Chem.* **1969**, *3*, 149-167.

[39] G. D. Purvis, R. J. Bartlett, *J. Chem. Phys.* **1982**, *76*, 1910-1918.

[40] T. H. Dunning Jr, *J. Chem. Phys.* **1989**, *90*, 1007-1023.

[41] F. Furche, R. Ahlrichs, *J. Chem. Phys.* **2002**, *117*, 7433-7447.

[42] D. C. Comeau, R. J. Bartlett, *Chem. Phys. Lett.* **1993**, *207*, 414-423.

[43] a) J. A. Sonk, H. B. Schlegel, *J. Phys. Chem. A* **2011**, *115*, 11832-11840; b) V. Riffet, D. Jacquemin, E. Cauet, G. Frison, *J. Chem. Theory Comp.* **2014**, *10*, 3308-3318; c) F. Turecek, *J. Phys. Chem. A* **2015**, *119*, 10101-10111.

[44] M. Barbatti, A. J. Aquino, H. Lischka, *Phys. Chem. Chem. Phys.* **2010**, *12*, 4959-4967.

[45] M. Barbatti, M. Ruckenbauer, F. Plasser, J. Pittner, G. Granucci, M. Persico, H. Lischka, *Wiley Interdisciplinary Reviews: Computational Molecular Science* **2014**, *4*, 26-33.

Entry for the Table of Contents (Please choose one layout)

Layout 1:

FULL PAPER

All mixed up: The cytosine radical cation ($Cyt^{\bullet+}$) is present as a mixture of several low-energy amino-type tautomers in the gas phase when formed via dissociation from the ternary Cu(II) complex. Specific isomers are distinguished via inspection of IR and UV action spectroscopy techniques, ion-molecule reactions, and theoretical calculations.

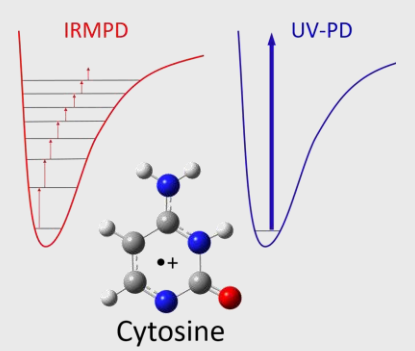

Michael Lesslie, John T. Lawler, Andy Dang, Joseph A. Korn, Daniel Bím, Vincent Steinmetz, Philippe Maitre, Frantisek Tureček and Victor Ryzhov**

Page No. – Page No.

Cytosine radical cation: a gas-phase study combining IRMPD spectroscopy, UV-PD spectroscopy, ion-molecule reactions, and theoretical calculations